An Objective Method for Measuring Surface Ice Accretion

PAUL TATTELMAN

Air Force Geophysics Laboratory, Hanscom AFB, MA 01731

(Manuscript received 3 September 1981, in final form 4 January 1982)

ABSTRACT

An off-the-shelf ice detection system used primarily on aircraft was tested in a climatic chamber, and then in the field to evaluate its ability to estimate the amount of ice simultaneously accreting on various-sized cylinders. The climatic chamber test data indicate that the system output is highly correlated with the mass and thickness of the ice measured on cylinders. A method, developed for utilizing the system for objectively estimating ice accretion amounts on cylinders, based on the chamber test results, is presented. Subsequent field tests indicate the system would be excellent for objectively estimating icing amounts on a cylinder for in-cloud icing on mountaintops. A slight modification is necessary to best use the instrument to estimate icing amounts from freezing rain or drizzle. Relationships of ice accretion characteristics on cylinders 3, 13, 25 and 50 mm in diameter for differing synoptic conditions are also discussed.

1. Introduction

In this report, ice accretion, or icing, refers to ice accumulating on stationary objects located near the earth's surface. It can totally disrupt transportation, cause power and communication outages, and result in severe damage to structures bearing the burden of accumulated ice. A primary concern to the United States Air Force is the design of structures such as radar and communication towers. Yet icing is one of the few meteorological conditions not quantitatively observed on a routine basis by any national weather service. Standardized icing measurements taken in conjunction with conventional weather observations would improve forecasts of icing amounts. Data collected could be used to develop refined estimates of icing amounts for structural design and deployment.

Most of the current information on ice storms was recorded only because of extensive human distress, or a large amount of damage. Even then, measurements have usually been made on tree branches, transmission lines, or just about any other convenient surface. These types of observations, which are subjective, nonstandardized, and difficult to interpret, were analyzed for the United States by Tattelman and Gringorten (1973). Bennett (1959) presented some standardized measurements taken by utilities and railroads in his comprehensive study of glaze. The most nearly objective measurements have been made using a cable suspended between two poles with a weight-measuring device, or tensionometer, between one of the poles and the cable. This method has been used to collect data in the Soviet Union (Rudneva, 1961). The Bonneville Power Administration, Portland, Oregon has many years of this type of data taken in mountain locations in the northwestern United States. Two shortcomings of this instrumentation that preclude its use at most observing sites are size and orientation, which result in ice amounts being a function of wind direction.

Due to the lack of data, some investigators, such as Lenhard (1955) and McKay and Thomson (1969), devised techniques for estimating ice amounts from readily available climatological data. To fulfill the Air Force need for reliable icing measurements for design, a program was initiated to develop a climatology of ice accretion. The first step toward this goal was the development of an objective method for measuring ice accretion.

2. Dynamics of ice accretion

There are three basic kinds of ice formed by accretion in the atmosphere: glaze, hard rime and soft rime. Glaze is transparent and is often referred to as clear ice. It has a density with respect to water (units for densities are g cm^{-3}) of 0.8 to 0.9 (the density of pure ice is 0.917). Hard rime is less transparent than glaze, and at times opaque, depending on the quantity of air trapped in the ice. The density varies from ~0.6 to 0.9. Soft rime is white and opaque. It is feathery or granular in appearance, with a density less than 0.6.

The adhesive strength of accreted ice on a surface is greatest when the density of the ice is high; this is because more particles are in contact with the surface. Consequently, the adhesive strength of both glaze and hard rime is high, but as the ice density decreases below about 0.6, its adhesive strength be-

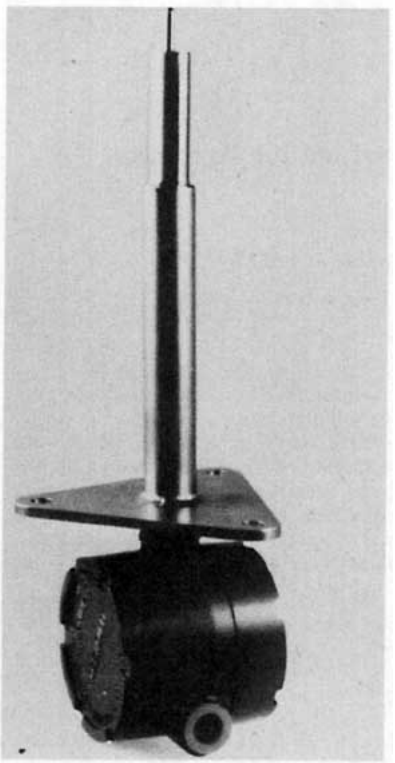

FIG. 1. The Rosemount Model 872DC Ice Detector. The sensing probe sits atop the 25.4 cm (10 in.) strut. During de-icing, the sensor and the top 7.6 cm (3 in.) of the strut are heated.

comes low enough for the ice to be shaken loose by a slight shock. Kuroiwa (1965) presents a more elaborate discussion on types of icing.

The most significant meteorological parameters which interact to determine the type of icing are: drop size, temperature, windspeed and liquid water content per unit volume of air. Macklin (1961) determined experimentally that ice density increases with an increase in each of these as long as the ambient temperature remains below freezing.

Raindrops with diameters greater than ~0.5 mm and with a maximum of ~5–6 mm will almost always produce glaze. Two main reasons are: 1) large drops cool more slowly upon impact with an object so that less air is trapped in the ice; and 2) freezing rain occurs at relatively high temperatures, rarely below −5°C (Bilello, 1971). Drizzle drops, which have diameters between ~0.2 and 0.5 mm, usually produce either glaze or hard rime. Freezing drizzle has been observed at much colder temperatures than freezing rain so that the density of accreted ice can vary more, depending upon the air temperature and windspeed.

Cloud or fog droplets have diameters <200 μm, but drops in the 100–200 μm range are rare except in clouds that are likely to precipitate. A review of cloud droplet sizes measured experimentally by Mason (1971) indicates that fog and stratus clouds have droplet sizes in the 1–45 μm range. Consequently, exposure to supercooled clouds or fog will usually result in soft rime. However, a combination of high windspeeds, temperatures just below freezing, and a high liquid water content can produce either glaze or hard rime.

Ice accretion measurements are extremely difficult to quantify because of the significant effect of size, shape and orientation with respect to air flow of the accreting object. This is because air is deflected around objects in its path, which influences the trajectories of supercooled drops in the flow. Basically, two factors act on the drops: drag and inertia. The drag on a drop's surface will tend to make the drop move with the air flow, but its inertia will tend to make the drop move in a straight line. As the drop size increases, the inertial effect increases faster than the drag effect because the volume, or mass, increases faster than the surface area. The larger the accreting object, the more it deflects the air ahead of the object, so that fewer drops per unit area impinge on larger objects than on smaller objects.

The term "collection efficiency," used to describe the effect of drop deflection, is defined as the ratio of the mass of drops impinging on an object in unit time to the mass of drops that would have impinged in the same time if there was no deflection. The collection efficiency increases as obstacle size decreases, and drop size increases.

3. The Rosemount ice detector

Sophisticated ice detectors have been developed for specific uses such as detecting icing on highways, runways and aircraft. Tests of some of these are discussed by Ackley *et al.* (1973) and Hill (1973). Hill concluded that a detector manufactured by Rosemount, Inc., Minneapolis, Minnesota had the greatest potential as a meteorological instrument for the detection of icing.

Rosemount markets a line of ice detectors used primarily to detect ice formation in the intake portion of turbomachinery. These detectors are aerodynamically designed for use on aircraft, but they have been used to detect icing on towers. The ice detector works by the magnetostriction principle. An oscillator forces a small closed cylinder (the sensing probe) to vibrate longitudinally, parallel to its axis. It is driven at its resonant frequency when dry, but accretion of ice will cause a shift in resonance corresponding to the increase in mass adhering to the probe. After a small preset thickness of ice has accumulated, the sensor is de-iced.

The advantages of using a Rosemount ice detector for observation of ice accretion are: convenient size, durability and operation with limited human involvement. These advantages are quite attractive when compared to other methods and devices that have

been tried. It was decided to test Rosemount detectors under controlled conditions in a climatic chamber in order to evaluate its ability to measure ice accretion. Accordingly, four model 872DC ice detectors, a newer model than those tested previously, were purchased from Rosemount. The main reason for the choice of this model is the long strut to keep accumulations on the mounting plate from influencing the flow past the sensor (Fig. 1). It was also necessary to purchase a model 524H controller, kept remote from the detectors, to actuate the de-icing system. A multi-channel event recorder was used to count de-icing cycles.

The ice detectors were calibrated at the factory to emit an icing signal when 0.5 mm of ice has accumulated on the sensing probe; however, detectors with trip points up to 5 mm are available. The sensor is cylindrical with a hemispheric top and has a diameter of 6 mm and a length of 27 mm. Because of its geometry, it is a very efficient collector. Although the detectors were calibrated to de-ice at 0.5 mm, the actual amount of ice required to trip the de-ice signal varies slightly, depending on the density and distribution of ice on the sensor. After the trip point has been reached, the sensing probe and top 76 mm of the strut are de-iced by an internal heater. Seven seconds after the start of the de-icing cycle, the unit is ready to begin the next sensing cycle.

Although we obtained an event recorder to use the discrete output (that is, count the number of de-icing cycles), a dc voltage recorder can be used to obtain an analog voltage output that will show the change in current as ice builds up on the sensor. It should be noted that light coatings of oil, dust, water, or other materials do not significantly affect operation of the ice detector.

4. The climatic chamber tests

Testing of the Rosemount ice detectors was conducted in May 1977 and January 1978 at the McKinley Climatic Laboratory of the Armament Development and Test Center (ADTC), Eglin AFB, Florida. Because of initial problems with the model 872DC detectors, model 871FA detectors, which differ only in configuration and strut length (5 cm), were used. Therefore, this article concentrates on the second test period, although Tattelman (1979) gives detailed information on all aspects of both test periods.

Two model 872DC detectors and one model 871FA detector were mounted on a stand. Measurements of ice thickness and mass were made on four horizontal cylinders, 3, 13, 25 and 50 mm in diameter located 30.5 cm behind and 15.2 cm above the sensors on the ice detectors. The cylinders were removable so that the mass of accreted ice could be determined. Room was not available to include vertically oriented cylinders, but previous icing tests by Stallabrass and Hearty (1967) indicate that, in spite of small differences in the shape of the ice accretion as a result of gravity affecting the run-off on a vertical cylinder, no difference in collection efficiency is apparent.

A total of 42 one-hour tests were run in the main chamber, which has floor dimensions of 61 × 77 m. Half of the tests simulated freezing rainfall rates of $\sim$1.27 and 2.54 mm h^{-1}, at temperatures from -1 to -7°C, and wind speeds of 5–35 knots. The other tests simulated in-cloud icing with $\sim$0.1 and 0.2 g m^{-3} water content, temperatures of -1 to -10°C, and wind speeds of 15–35 knots. Additional longer-duration tests, some with varying conditions, were also run.

The wind was created using a large electric fan. Windspeed, which was measured at the test stand using a hand-held 3-cup anemometer, was adjusted by the distance of the fan from the stand. Elaborate spray rigs were used to produce freezing rain and in-cloud icing conditions with nozzles chosen to simulate natural drop size distributions for both conditions. Water temperature was regulated to be as close to freezing as possible at the time it left the nozzles, and ambient air temperature was continually monitored. Tattelman (1979) provides details on controls over tests, which were intended to simulate icing within the range of natural synoptic icing conditions. However, the validity of the tests depended more on our efforts to ensure the uniformity of icing in the area occupied by the detectors and cylinders.

5. Analysis of test results

At the conclusion of each test, measurements were made of the maximum radial ice thickness (the maximum ice thickness on the cylinder regardless of orientation), the vertical ice thickness (the total thickness of ice in the vertical, both above and below the cylinder, excluding icicles), and the mass of ice on each of the four cylinders. The color and shape of the ice formation were also noted. Measurements of ice density were not made because of problems in obtaining accurate measurements with the rotating cylinder that was tried during the original tests. The number of detector de-icing cycles was also recorded for each test.

a. Mass of ice

The regression lines and scatter of the individual test points for the mass of ice on the 25-mm diameter cylinder versus the number of cycles for detector 1 (one of the model 872DC detectors) are shown for all 42 1-h tests (Fig. 2), for the 21 freezing rain tests (Fig. 3), and for the 21 in-cloud icing tests (Fig. 4). There is little difference in scatter diagrams for the other two detectors. The results of the linear regres-

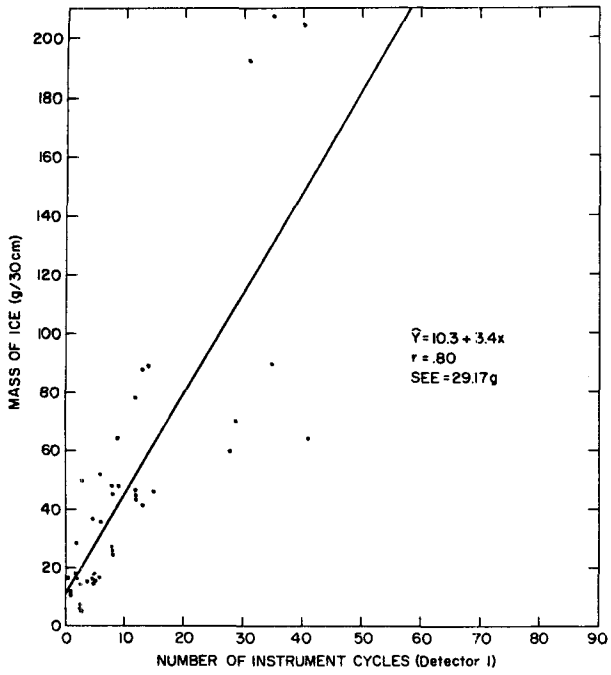

FIG. 2. Mass of ice on the 25-mm diameter cylinder vs the number of instrument cycles (detector 1) for all 1-h tests.

sion analysis for the mass of ice on the 3-, 13-, and the 50-mm diameter cylinders (not presented) were very similar. The marked improvement in correlation and Standard Error of Estimate (SEE) that results from separating the in-cloud icing and freezing rain data is obvious.

For a specific number of detector cycles, a much greater mass of ice would accumulate on the cylinder during freezing rain than during in-cloud icing. This can be seen in Fig. 5, which shows the regression lines of the mass of ice on the 3- and 25-mm diameter cylinders versus the number of detector cycles for detector 1. The difference in the regression lines can be best explained by considering the freezing fraction, that is, the ratio of the amount of ice that actually freezes on the collector to that amount which would accumulate if all the drops impinging on the collector freeze. During in-cloud icing, drops freeze quickly to the collector since the heat loss, especially the transfer of latent heat from the freezing of these small drops, is relatively rapid. The larger drops, during freezing rain, freeze more slowly. This allows part of the water to run off or be blown off the surface. Stallabrass and Hearty (1967) found that the freezing fraction is influenced by the ambient temperature and the water concentration. With these factors being equal, a larger surface area will allow a greater proportion of the impinging drops to freeze. This is primarily due to the increased time the drops remain on the surface, and the larger ice surface to which heat can be imparted. It seems likely that, during freezing rain, many of the drops impinging on the sensor will splatter, run off, or be blown off due to its smaller 6-mm diameter, whereas they are retained on the 25-mm diameter cylinder. The rap-

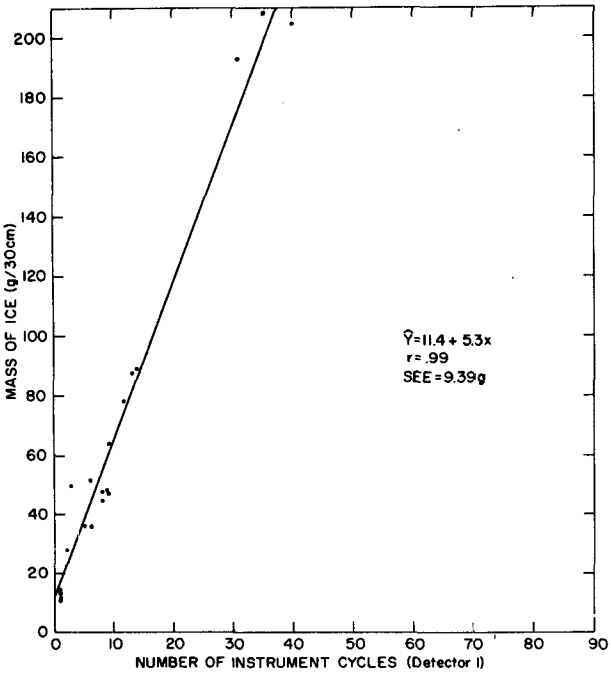

FIG. 3. Mass of ice on the 25-mm diameter cylinder vs the number of instrument cycles (detector 1) for the 21 freezing rain tests.

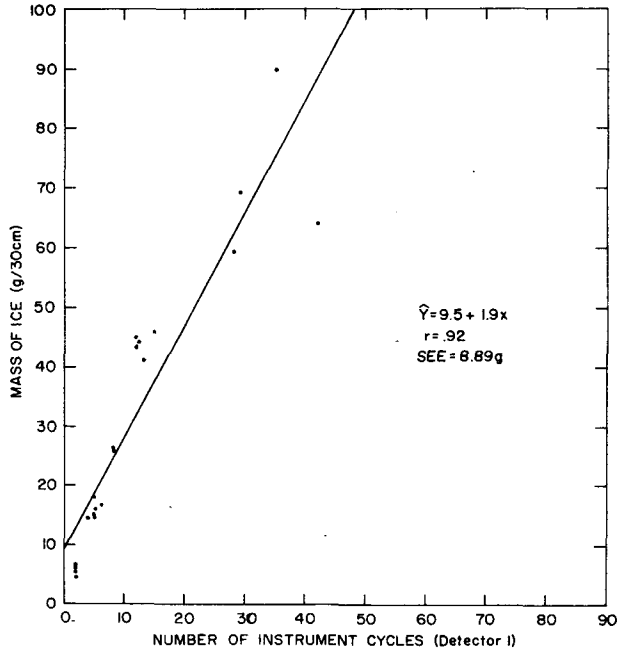

FIG. 4. Mass of ice on the 25-mm diameter cylinder vs the number of instrument cycles (detector 1) for the 21 in-cloud icing tests.

idly expanding ice surface on the 3-mm cylinder will gradually allow a larger percentage of these drops to freeze.

b. *Maximum radial ice thickness*

Linear least-squares regression lines of the maximum radial ice thickness (MRIT) on the 25-mm diameter cylinder versus the number of instrument cycles, and scatter of the individual points, for all tests, for the 21 freezing rain tests, and for the 21 in-cloud icing tests for detector 1 are shown in Fig. 6. They indicate that the fit of the regression line is improved by separating the freezing rain and in-cloud icing tests. However, the improvement is not as obvious as for the mass of ice. Fig. 7 shows a comparison of the least-squares regression lines of the 3- and 25-mm diameter cylinders for the MRIT versus the number of instrument cycles. During in-cloud icing, the ice thickness is greater for the 3-mm cylinder as to be expected from icing theory. During freezing rain, however, the ice thickness is slightly greater on the 25-mm cylinder. The implication here is that the theoretical relationship of the collection efficiency of objects of different sizes is limited by the drop size; that is, once drops reach a certain volume or mass, their inertia is great enough so that the drag effect is not sufficient to deflect a significant number of these large drops.

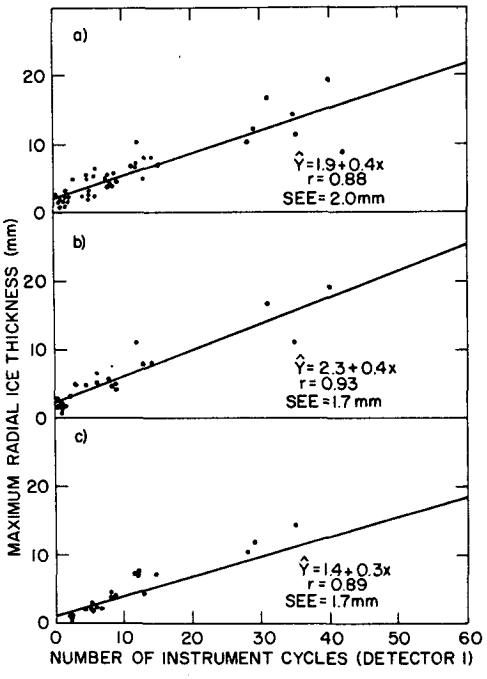

FIG. 6. Maximum radial ice thickness on the 25-mm diameter cylinder vs the number of instrument cycles (detector 1): (a) for all 42 one-hour tests; (b) for the 21 freezing rain tests; (c) for the 21 in-cloud icing tests.

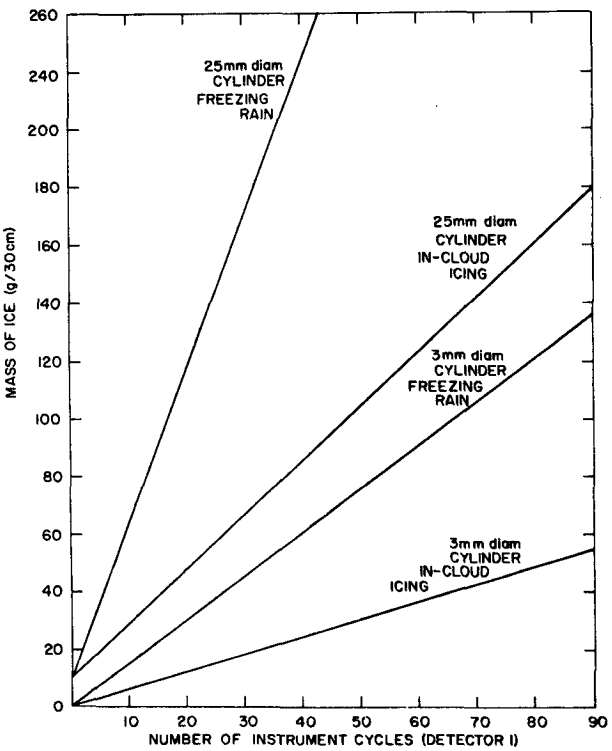

FIG. 5. Least-squares linear regression lines of the mass of ice on the 3- and 25-mm diameter cylinder vs the number of instrument cycles (Detector 1) for the freezing rain and in-cloud icing tests separately.

c. *Vertical ice thickness*

Fig. 8 shows the least-squares linear regression lines of the vertical ice thickness (VIT) versus the number of instrument cycles for detector 1. The results were very similar for the other two detectors. Fig. 8 indicates that during freezing rain the accreted ice adds to the vertical dimension on all four cylinders. Also, the smaller cylinder diameters generally favor more vertical growth. During in-cloud icing the same trend is evident. However, both the 25- and 50-mm cylinders experience negligible vertical growth. These results indicate that, during freezing rain, the large drops are not easily deflected, even by the 50-mm diameter cylinder. During in-cloud icing, the small droplets are deflected much more with increasing cylinder diameter. Consequently, vertical growth of the ice is less important during in-cloud icing than during freezing rain.

d. *Long-duration tests*

In order to study more completely the performance of the ice detectors, six climatic chamber tests were run with durations from 2 to 17 h, some with varying conditions. Test conditions and results are contained in Table 1. As a result of these longer tests, a major problem area was uncovered. During the 15- and 17-

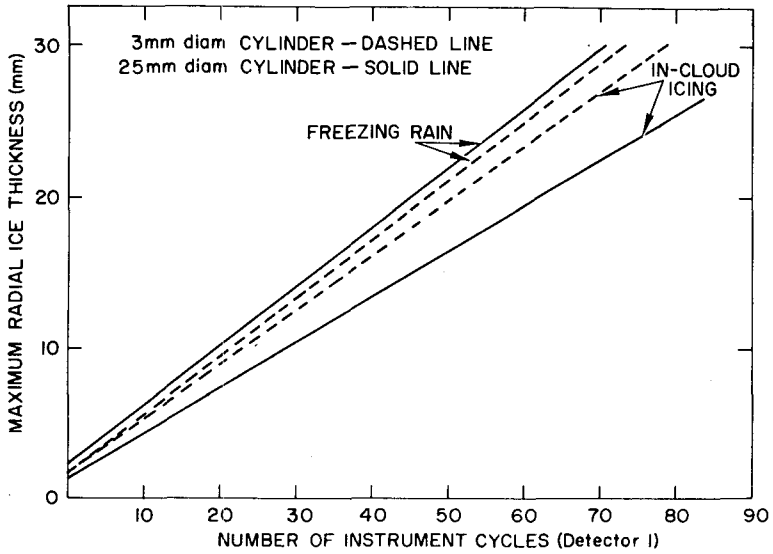

FIG. 7. Least-squares regression lines of the maximum radial ice thickness on the 3- and 25-mm diameter cylinders vs the number of instrument cycles (detector 1) for the freezing rain and in-cloud icing tests separately.

h freezing rain tests (test numbers 5 and 6), the detectors cycled erratically even though synoptic conditions remained unchanged. This was caused by melt water from the sensor accumulating on the flat surface area on the top of the strut, and held in place by surface tension. During test 6, with the temperature at −4°C, the puddle froze rapidly. The sensor, which was partially submerged in the puddle, responded by returning to the de-ice mode. This accounts for the large number of cycles for detectors 1 and 3 in this test. Because of the narrow strut on detector 2 (Model 871FA), melt water drained more readily and no puddle formed.

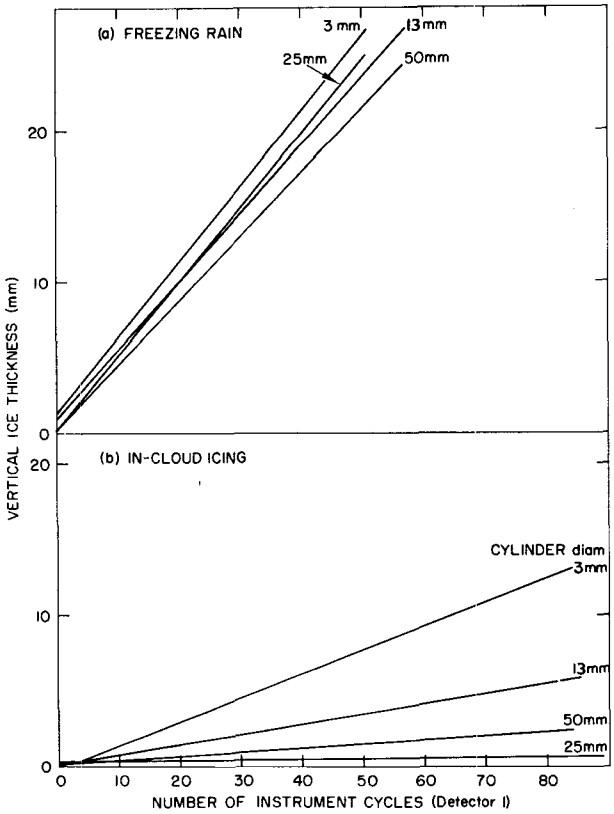

FIG. 8. Least-squares regression lines of the vertical ice thickness vs the number of instrument cycles (detector 1) for: (a) freezing rain; (b) in-cloud icing.

During test 5, with the temperature at −1°C, the puddle was slow to freeze. It is not apparent what physical effect this had on the cycling of the detector. Although de-icing intervals were irregular, excessive cycling did not occur as in test 6. Fig. 9 shows the least-squares linear regression lines for the mass of ice on the 25-mm diameter cylinder versus the number of instrument cycles, from the climatic chamber 1-h tests, for each detector. The values for the mass of ice on the 25-mm diameter cylinder versus the number of cycles for each detector in the long-duration tests (Table 1) are plotted. Since the number of cycles for detectors 1 and 3 in test number 6 are not representative, they have not been plotted.

Table 2 contains the percentage difference between the mass of ice measured on the 25-mm diameter cylinder in the long-duration tests and that estimated from the regression lines for each detector. The percentage differences are notably larger for the freezing rain tests. Also, the regression lines for freezing rain underestimated the mass of ice in six of the seven cases. One explanation for this is the greater growth in the size of the cylinder plus ice, especially in the vertical plane, during freezing rain. As indicated previously, the larger the cylinder, the

TABLE 1. Results of long duration tests for in-cloud icing, tests 1–3, and for freezing rain, tests 4–6.

Test number	Conditions: Windspeed (kt)	Temperature (°C)	Cloud liquid water content (g m^{-3})	Duration (h)	Mass of ice on the 25 mm diam. cylinder [g (30 cm)$^{-1}$]	Number of cycles: Detector and Model 1 872DC	2 871FA	3 872DC
1	15	−4	0.2	½				
	15	−4	0.1	½				
	25	−4	0.1	½				
	25	−4	0.2	½				
			Total	2	34.5	9	10	7
2	15	−4	0.1	1				
	15	−7	0.1	1				
	15	−7	0.2	1				
	25	−7	0.1	1				
	25	−10	0.2	1				
	35	−10	0.2	1				
			Total	6	122.8	61	68	64
3	15	−4	0.2	6	64.5	23	30	21
			Rain Rate (mm h^{-1})					
4	5	−4	2.54	1				
	5	−1	2.54	1				
	15	−1	2.54	1				
	15	−4	2.54	1				
	25	−4	1.27	1				
			Total	5	308.6	34	37	29
5	5	−1	2.54	15	539.0	39	40	58
6	5	−4	1.27	17	156.6	115	28	124

greater the mass of accumulated ice. Evidently, using the regression lines based on the 1-h tests can lead to significant underestimates of the mass of ice during prolonged severe icing such as our long duration tests. This is not a serious problem during in-cloud icing because vertical growth on the cylinder is small and the frontal projection remains effectively unchanged.

6. Application

The application of ice accretion measurements is primarily in the area of environmental design criteria. The two aspects of ice accretion that are important in design and operation of equipment are: 1) wind loading due to the increased surface area of the structure as a result of accumulated ice; and 2) the mass of ice on the structure.

An engineer must determine surface area to calculate the force of the design windspeed on a structure. This is straightforward when ice is not present, since the surface area can be easily calculated, and data on windspeed distributions are available for a large number of locations. When ice is present, the distribution of concurrent observations of windspeed and ice thickness must be known. During natural ice accretion, ice thickness varies and assumes a variety of shapes, depending on the orientation and size of the collecting surface and the synoptic conditions. This can be further complicated by the presence of icicles, which are not usually included in measurements of ice thickness.

During the climatic chamber tests, measurements were made of the ice thickness in the vertical as well as the maximum radial ice thickness. However, these measures of thickness are dependent on cylinder orientation relative to the wind direction. The term "radial ice thickness" has frequently been used in the literature to describe ice thickness (Tattelman and Gringorten, 1973). This term implies a uniform coating of ice on a cylinder such that the thickness of the ice is the radius of the cylinder and ice minus the radius of the cylinder. The concept is attractive in its simplicity, even though it does not describe the shape of accreted ice actually occurring in nature. This approach to ice thickness was explored using the data from the climatic chamber tests.

Consider a cylinder with length L and radius r_2. Let r_1 be the radius of cylinder plus a uniform coating of ice on the cylinder. Then

$$T = r_1 - r_2 \tag{1}$$

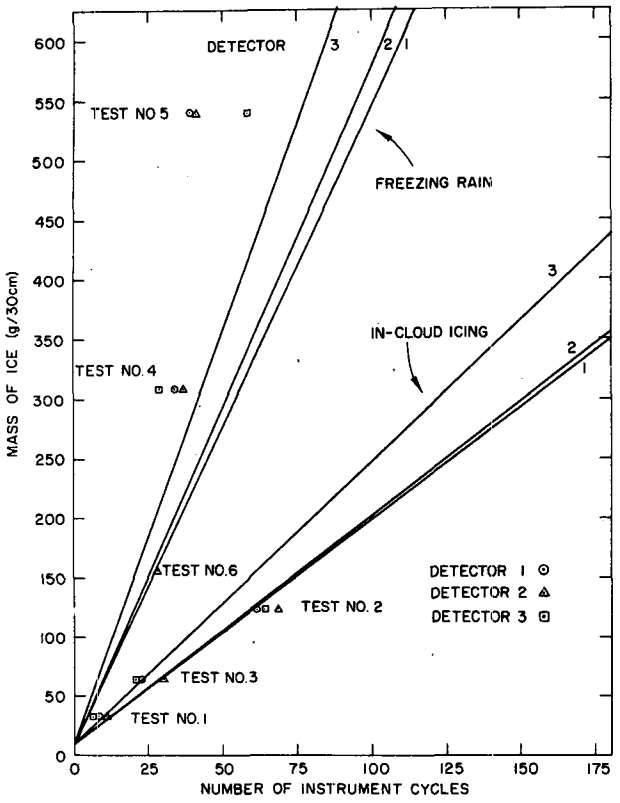

FIG. 9. Least-squares linear regression lines for the mass of ice on the 25-mm diameter cylinder vs the number of instrument cycles for each detector from the climatic chamber 1-h tests. Values for the long duration tests are outlined with a circle for detector 1, a triangle for detector 2, and a square for detector 3.

where T is the theoretical radial ice thickness. From simple geometry, the volume of ice V_I can be calculated from

$$V_I = \pi L(r_1^2 - r_2^2), \tag{2}$$

so that

$$r_1 = \left(\frac{V_I}{\pi L} + r_2^2\right)^{1/2}. \tag{3}$$

TABLE 2. Percentage difference between the mass of ice measured on the 25-mm diameter cylinder in the long duration tests and that estimated from the regression lines for each detector.*

Test number	Type of icing	Percentage difference Detector 1	2	3
1	In-cloud	30	25	35
2	In-cloud	−2	−12	−24
3	In-cloud	22	−3	9
4	Freezing rain	60	42	48
5	Freezing rain	46	29	31
6	Freezing rain	—	−6	—

* Negative sign indicates that the measured mass is less than that obtained from the regression line.

Also,

$$V_I = M_I/\rho_I, \tag{4}$$

where M_I is the mass of ice on the cylinder and ρ_I is the ice density. Combining Eqs. (3) and (4) and substituting for r_1 in Eq. (1), one obtains

$$T = \left(\frac{M_I}{\rho_I \pi L} + r_2^2\right)^{1/2} - r_2. \tag{5}$$

The actual increase in the thickness of the cylinder plus ice is $2T$. For a 25.4 mm diameter cylinder with a length of 304.8 mm, and assuming an ice density of 0.9 g cm^{-3}, the theoretical increase in the thickness (in cm) of the cylinder T' is

$$T' = 2\left(\frac{M_I}{86.2} + 1.61\right)^{1/2} - 2.54, \tag{6}$$

where M_I is in grams.

The least-squares linear regression of T', calculated using the mass of ice on the 25-mm diameter cylinder, versus the VIT on the same cylinder for the 21 freezing rain tests is shown in Fig. 10. Fig. 11 shows the least-squares linear regression of T' versus the MRIT for the same tests. These figures show that there is a significant relationship between T' and both the VIT and the MRIT. If Eq. (6) provided the best possible results, the regression lines in Figs. 10 and 11 would have an intercept of zero and a slope of 1; that is,

$$\hat{Y} = T'. \tag{7}$$

If we use 0.8 g cm^{-3} rather than 0.9 g cm^{-3} for the

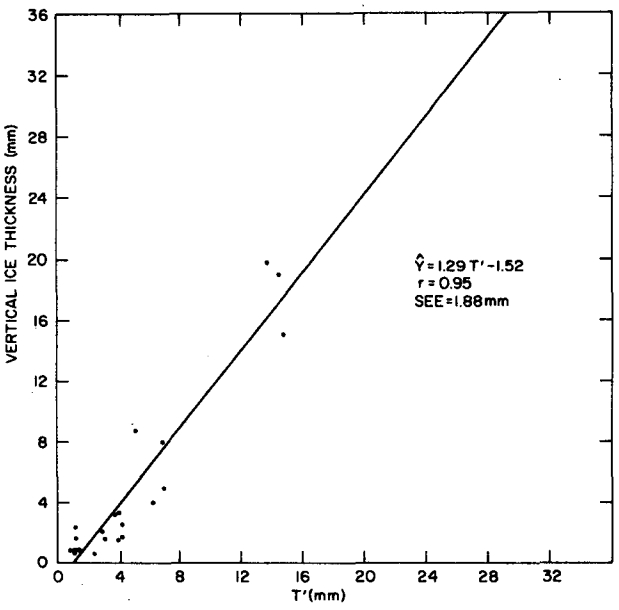

FIG. 10. Least-squares linear regression of the vertical ice thickness for the freezing rain tests vs T'.

ice density, then

$$T' = 2\left(\frac{M_I}{76.6} + 1.61\right)^{1/2} - 2.54, \qquad (8)$$

for the 25-mm diameter cylinder. The least-squares linear regression lines for T' calculated from Eq. (8) versus the VIT and the MRIT are shown in Fig. 12. Eq. (7), shown as a dashed line, provides a good estimate of the ice thickness. The use of 0.8 g cm^{-3} for the density of ice formed by freezing rain is reasonable, since there are usually some air bubbles trapped in the ice, and the actual density would be between 0.8 and 0.9 g cm^{-3}. The density of pure ice is 0.917 g cm^{-3}. Therefore, Eq. (8) can be used to calculate T' from the mass of ice on the 25-mm diameter cylinder due to freezing rain. Analyses of the ice thickness on the 3-, 13-, and 50-mm diameter cylinders with an ice density of 0.8 g cm^{-3} yielded similarly good results.

For in-cloud icing, a density of 0.6 g cm^{-3} was used in Eq. (5) resulting in the expression

$$T = \left(\frac{M_I}{57.4} + 1.61\right)^{1/2} - 1.27. \qquad (9)$$

This density is the approximate lower limit for hard rime, and its use will maximize the theoretical radial ice thickness calculated using Eq. (5). Ice with a lower density has little adhesive strength; it is not an important design consideration since it would be blown off by strong winds. The least-squares linear regression of T' versus the MRIT on the 25-mm diameter cylinder for the 21 in-cloud icing tests is presented in Fig. 13. Eq. (7) is also shown as a dashed line. For the same tests, the regression line for the VIT on the 25-mm diameter cylinder versus T' is not shown because the vertical thickness was close to zero, although some vertical growth occurred on the smaller (3- and 13-mm diameter) cylinders. The increased surface area due to the MRIT depends on the orientation of the ice-coated structure to the wind. The use of Eq. (9) to calculate T on the 25-

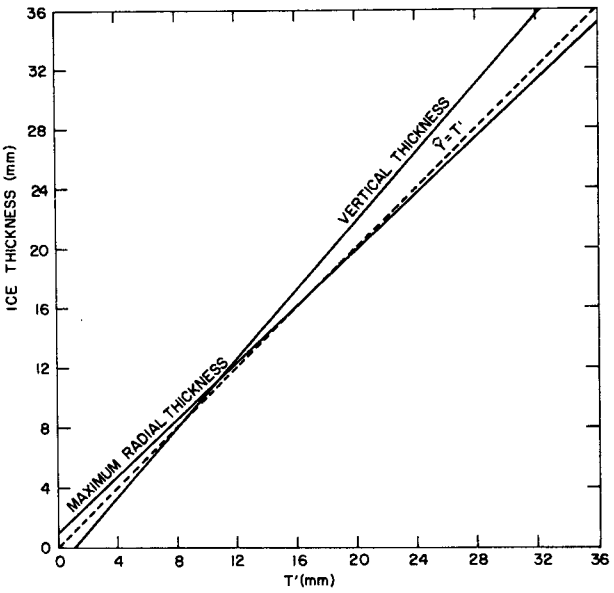

FIG. 12. Least-squares linear regression lines of the vertical ice thickness and the maximum radial ice thickness vs T' from Eq. (8) for the freezing rain tests. $\hat{Y} = T'$ is represented by the dashed line.

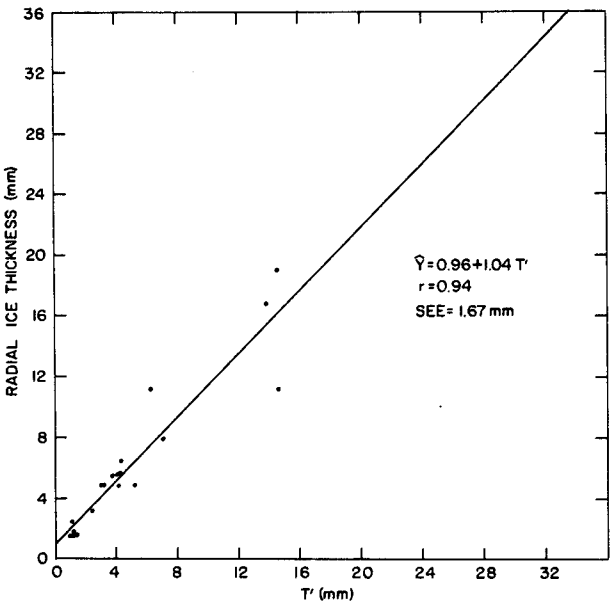

FIG. 11. Least-squares linear regression of the maximum radial ice thickness for the freezing rain tests vs T'.

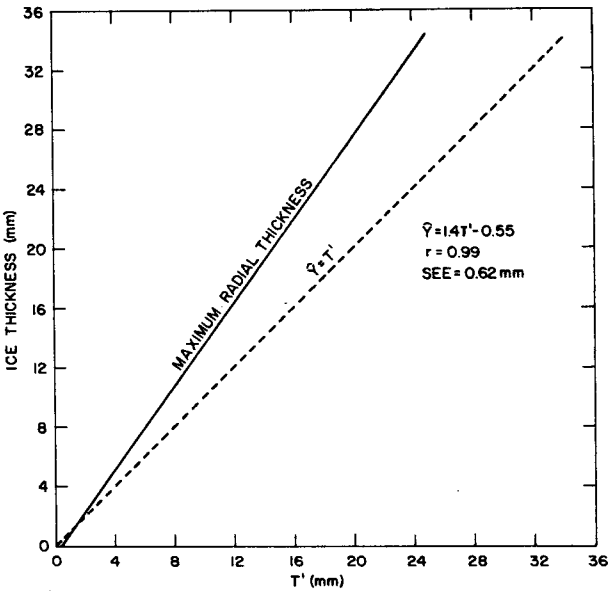

FIG. 13. Least-squares linear regression of the maximum radial thickness vs T' for the in-cloud icing tests. $\hat{Y} = T'$ is represented by the dashed line.

TABLE 3. Mean and standard deviation of the ratios of the mass of ice on the 3-, 13-, and 50-mm diameter cylinders to that on the 25-mm diameter cylinder.

Category	Cylinder diameter (mm/inches)	Mean	Standard deviation
In-cloud icing	3.2/⅛	0.21	0.059
In-cloud icing	12.7/½	0.59	0.062
In-cloud icing	50.8/2	1.47	0.116
Freezing rain	3.2/⅛	0.18	0.041
Freezing rain	12.7/½	0.54	0.056
Freezing rain	50.8/2	1.65	0.091
Both combined	3.2/⅛	0.20	0.054
Both combined	12.7/½	0.57	0.063
Both combined	50.8/2	1.56	0.139

mm diameter cylinder for in-cloud icing is a compromise for all possible orientations to the wind.

A suggested method for utilizing the output of the 872DC ice detector in the field would be to use the number of recorded deicing cycles to determine the mass of ice per unit length on a cylinder. If we adopt the mass of ice per 30.5 cm on the 25-mm diameter cylinder as a basis for describing ice accretion observations, then the mass of ice on the 3-, 13-, and 50-mm diameter cylinders can be determined using the ratios given in Table 3. T can then be calculated for each cylinder size using Eq. (5) with the appropriate ice density for the type of icing.

7. Field tests

a. Data collection

Rosemount Model 872DC ice detectors were mounted on a stand and installed at Hanscom AFB, Mass. in February 1979, Westford, Mass., Blue Hill Observatory, Milton, Mass., and the summit of Loon Mt., Lincoln, N.H., in November 1979. The elevation is <70 m at the Bedford and Westford sites, 190 m at the summit of Blue Hill, and 915 m at the summit of Loon Mt. A cylinder 25 mm in diameter, and 30.5 cm in length, selected as the standard for our observations, was mounted on a wind vane colocated on the stand with the ice detector. The cylinder is kept normal to the wind flow by the vane to standardize thickness measurement; it can be removed to determine the mass of the ice. The distance between the vane and the ice detector is ~1 m.

At the conclusion of each icing event, the MRIT, the VIT, the mass of the ice, the appearance of the ice, and information on icicles was recorded. Synoptic weather conditions for the period of icing were also noted. At the completion of data collection, the cylinder was cleared of ice and placed back on the vane. For each event, the analog output of the ice detectors was recorded in addition to the number of heating cycles. This was done to observe the detector response to ice on the sensor between the no-ice condition and the trip point, when the heater activates.

Much of the information collected is summarized in Table 4. Columns headed by $\hat{M}_c$, $\hat{M}_r$, $\hat{T}_c$ and $\hat{T}_r$ are estimated values of the mass (M) and thickness (T) based on the climatic chamber test data. Data for all three detectors used in the chamber tests were pooled to smooth out the differences in their response before developing linear least-squares regression lines of the number of de-icing cycles versus the mass of ice on a 25-mm diameter cylinder per 30.5 cm length. The resulting equations are

$$\hat{M}_r = 9.1 + 5.8N, \tag{10}$$

and

$$\hat{M}_c = 9.4 + 2.0N, \tag{11}$$

where $\hat{M}_r$ and $\hat{M}_c$ are estimates of the mass of ice

TABLE 4. Summary of icing events, associated weather, ice measurements, and the number of de-icing cycles. $\hat{M}_c$, $\hat{M}_r$ and $\hat{T}_c$, $\hat{T}_r$ are estimates of the mass and thickness, respectively, of ice on the cylinder based on previous climatic chamber tests.*

Location	Event number	Date	Duration of event (h, min)	Weather	Max. temp. (°C)	Min. temp. (°C)	Wind direction	Mean speed (kt)
Blue Hill	1	10 Oct 79	5 0	S, F	0.0	−0.6	NNE-NNW	9
	2	13 Dec 79	7 30	S, F	−0.6	−0.6	NE	14
	3	13-14 Dec 79	7 45	ZR, ZL, S	0.0	−5.6	NE-NNW	13
	4	17 Jan 80	11 0	ZL	−3.3	−6.1	N-NNW	14
	5	17-18 Jan 80	18 33	ZL, F	−0.6	−3.3	N-NNW	9
	6	22 Feb 80	4 27	ZL, ZR, F	−0.6	−2.8	E-ESE	12
Hanscom AFB	7	26-27 Feb 79	15 0	ZR	NA	NA	NA	NA
	8	17-18 Jan 80	7 30	ZL	NA	NA	NA	NA
	9	22 Jan 80	6 0	S, ZR	0.0	−1.1	Variable	2
	10	22 Feb 80	7 30	ZR, ZL	0.0	−2.2	Variable	3
Westford	—	18 Jan 80	3 0	ZL	−0.6	−1.7	NNE	3
	11	22 Feb 80	5 25	ZR, ZL	0.0	−1.4	ENE	5

* Subscript c denotes estimate for in-cloud icing, subscript r denotes estimate for freezing rain. NA: Not available. S: Snow. ZR: Freezing rain. ZL: Freezing drizzle. F: Fog.

for freezing rain and in-cloud icing, respectively, and N is the number of detector de-icing cycles. The correlations and SEE's are 0.98 and 13.3 g for Eq. (10), and 0.92 and 9.0 g for Eq. (11).

The estimates of ice thickness in Table 4 are represented by $\hat{T}$, where

$$\hat{T} = T' = 2T. \tag{12}$$

The estimated thickness is twice the theoretical radial ice thickness T from Eq. (5), since the actual increase in the thickness of the cylinder plus ice is twice the theoretical radial ice thickness. For a cylinder radius of 12.7 mm, a length of 304.8 mm, and using an ice density of 0.8 for ice formed by freezing rain and a density of 0.6 for in-cloud icing, Eq. (12) becomes

$$\hat{T}_r = 2\left(\frac{M_I}{76.6} + 1.61\right)^{1/2} - 2.54, \tag{13}$$

$$\hat{T}_c = 2\left(\frac{M_I}{57.4} + 1.61\right)^{1/2} - 2.54, \tag{14}$$

where $\hat{T}_r$, the estimated thickness due to freezing rain, and $\hat{T}_c$, the estimated thickness due to in-cloud icing, are in centimeters and M_I is in grams.

The information on the type of weather in Table 4 shows that, frequently, a variety of conditions combine to produce icing. Therefore, for each icing event, estimates were made of the mass and thickness of ice for both freezing rain and in-cloud icing. These two types of icing represent the upper and lower limits of drop sizes that produce natural icing. The optimum result would be to have the measured mass of ice on the cylinder, for the mixed icing or freezing drizzle icing events, fall between the freezing rain and in-cloud icing estimates. A good estimate of the thickness for an icing event would fall between the MRIT and the VIT.

b. Analysis

Table 4 provides information on 12 icing events. Unfortunately, it was a dry winter at Loon Mt and no usable data were collected there. For the 18 January event at Westford, the ice accumulation was not sufficient to produce any detector cycles. Fig. 14 shows the regression lines for $\hat{M}_r$ and $\hat{M}_c$; also shown are circled points for the measured mass of ice on the cylinder for the remaining 11 icing events. Each point is identified by the event number in Table 4.

Six of the 11 points in Fig. 14 fall between the regression lines. Two of the five events not within the regression lines (numbers 1 and 2) were the result of wet snow. Two other events, numbers 3 and 9, had some snow mixed in. Although the ice detector response to wet snow is not known, this small sample indicates that the mass build-up of ice on the cylinder per instrument cycle may be less than that for in-cloud icing. Although an effort was made to measure icing amounts at the conclusion of an event, it was not always possible to tell if icing had ceased, and on some occasions the observer could not be present at the conclusion of icing. The elapsed time between the end of icing until the icing amounts on the cylinder were observed is given in Table 4. Events 3, 8, and 9 were the only instances where more than 1 h elapsed before the observation was made. Even though temperatures remained at or below freezing during this period, some loss of ice on the cylinder, due to melting or evaporation, was likely. Therefore, all of the points below the in-cloud icing regression line in Fig. 14 represent icing events which either involved snow and/or a substantial period before observation, allowing for potential ice loss.

The icing events included some other interesting aspects. For instance, icicles did not form during any of the events. Also, the two heaviest icing periods (events 4 and 5) occurred with only 0.8 mm (0.03

TABLE 4. (*Continued*)

Melted precipitation (mm)	MRIT (mm)	VIT (mm)	Mass of ice (g)	Number of detector cycles	$\hat{M}_c$ (g)	$\hat{M}_r$ (g)	$\hat{T}_c$ (mm)	$\hat{T}_r$ (mm)	Time between end of icing until observation (h, min)
NA	1.6	0	10.6	3	15.4	26.5	2.0	2.6	0 0
9.7	0.2	0	1.1	6	21.4	43.9	2.8	4.2	0 0
4.6	4.6	2.0	22.9	8	25.4	55.5	3.2	5.2	7 45
0.8	9.7	2.9	68.7	11	31.4	72.9	4.0	6.6	0 0
0.5	7.9	1.6	55.0	11	31.4	72.9	4.0	6.6	0 0
1.5	6.4	2.7	46.5	10	29.4	67.1	3.7	6.1	0 0
NA	1.6	1.6	30.3	4	17.4	32.3	2.3	3.1	1 0
NA	0.3	0.1	4.4	3	15.4	26.5	2.0	2.6	2 30
NA	1.4	1.4	6.6	2	13.4	20.7	1.8	2.0	13 15
NA	5.2	2.2	24.6	6	21.4	43.9	2.8	4.2	0 0
Trace	<0.1	<0.1	2.0	0	—	—	—	—	—
NA	3.8	3.8	24.5	5	19.4	38.1	2.5	3.6	0 40

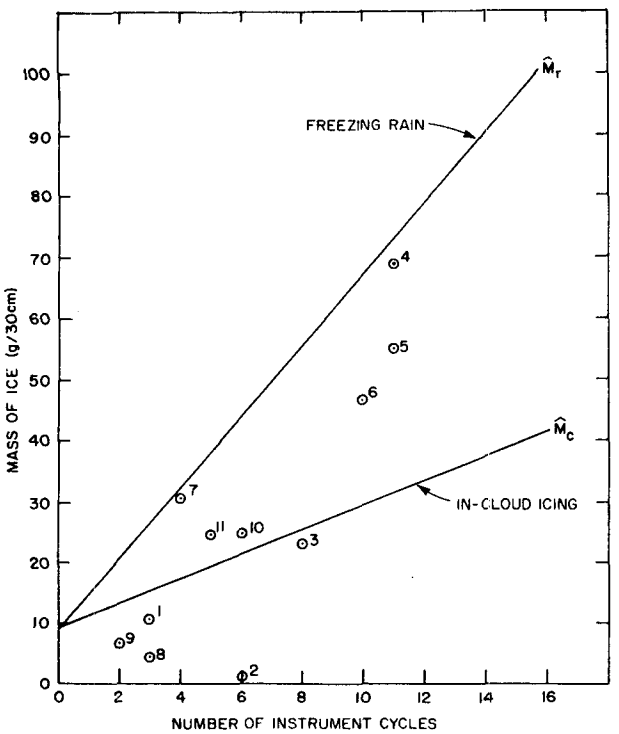

FIG. 14. Regression lines for the mass of ice measured on the 25-mm diameter cylinder vs the number of instrument cycles for freezing rain $\hat{M}_r$, and for in-cloud icing $\hat{M}_c$, based on the climatic chamber tests. Circled points represent the mass of ice measured on the cylinder vs the number of cycles for the field test icing events. Event numbers from Table 4 identify each point.

in) and 0.5 mm (0.02 in) of melted precipitation, respectively. Both events were part of a static synoptic situation with drizzle, separated by a period of time with no precipitation. Unfortunately, no in-cloud icing occurred, except at Blue Hill (events 1 and 2) when the bulk of resulting ice was caused by wet snow which formed a slush that froze.

To get an appreciation of our method for determining the ice thickness, Fig. 15 compares the theoretical ice thickness curves from Eqs. (13) and (14) along with the plotted values of the actual mass of ice versus the average of the VIT and the MRIT for each icing event. Most of the icing events were the result of a mixture of conditions that could not be strictly categorized as either in-cloud icing or freezing rain. Ideally the points would lie on, or between, the two lines. Since only one event (number 7) is not close to or between the curves, these results indicate that the radial ice thickness approach will provide reasonable estimates of ice thickness based on the mass of ice.

Examination of the information in Table 4 and Fig. 14 leads one to support the potential of the Rosemount 872DC ice detection system as a network instrument for making objective observations of ice accretion. Additional data needs to be collected, perhaps in a climatic chamber, to establish regression lines for freezing drizzle or mixed icing that would fall between those for freezing rain and in-cloud icing.

c. *Equipment problems*

The optimism expressed in the preceding section is tempered by two problems, water retention on the flat surface between the ice detector strut and the sensor, and instrument calibration. The problem of water retention on the strut was originally noted at the time of the chamber tests. During the heating cycle, melt water from the sensor flows down to the flat surface of the top of the strut. Surface tension keeps the liquid in place and it freezes. With subsequent de-icing cycles, the melt water can eventually surround the sensor in a puddle deep enough to automatically trip the de-ice mode, even though the actual icing may have stopped. This occurred during prolonged icing tests with winds less than ~15 knots. When the wind was stronger, the melt water was blown off. It was not a problem during the in-cloud icing tests which had winds of at least 15 knots.

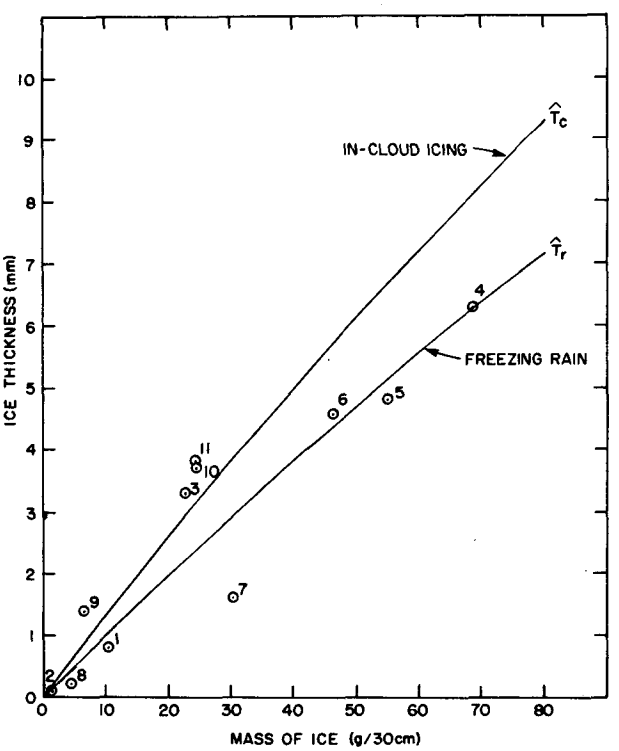

FIG. 15. Ice thickness curves for in-cloud icing $\hat{T}_c$ and for freezing rain $\hat{T}_r$, vs the mass of ice on the 25-mm diameter cylinder. Circled points represent the average of the MRIT and the VIT vs the actual mass of ice measured on the cylinder for each icing event. Event numbers from Table 4 identify each point

Excessive instrument cycling due to freezing melt water occurred during two of the field test icing events, numbers 5 and 11. These were corrected to the number of cycles shown in Table 4 by analyzing the recorded analog output for the distinctive shape of the erroneous cycle. It was found that this response could be artificially duplicated by spraying the sensor with an atomizer through several de-icing cycles until the melt water reached the critical depth. At that point, the instrument would cycle on its own every time the puddle froze. Tilting the detector did not facilitate the flow of water from the top of the strut until its angle from the vertical was >60°. Positioning the strut at this angle would not be a viable solution, since the instrument response would become a function of wind direction. The most practical way to eliminate this problem would be to taper the top of the strut to facilitate drainage. Representatives at Rosemount indicated that this could be accomplished, but with additional cost.

The ice detectors were returned to Rosemount for evaluation at the conclusion of the winter field tests. When purchased in March 1977, the ice detectors were calibrated at the factory to de-ice (reach the trip point) when 0.51 mm (0.02 in) of ice accumulated on the sensor. Rosemount found that the detector used at Westford was only slightly out of calibration with a trip point of 0.53 mm. The Hanscom and Blue Hill detectors, however, were substantially out of calibration with trip points of 0.44 and 0.39 mm, respectively. Rosemount was unable to determine cause, but noted that the sensors on these two detectors were discolored. They thought that this was probably caused by overheating, causing a material stress which affected the calibration. The discoloration was not present at the conclusion of the climatic chamber tests, but it did become apparent at the beginning of the field tests. It might have been caused by an extended period with the heater on while testing the initial installation in the field. The obvious change in color would at least signal the need for recalibration if this happened during actual use of the detector for icing observations.

The change in calibration was <5% for the Westford and Loon Mt. detectors. For the Blue Hill and Hanscom detectors, the respective changes in calibration of 24 and 14% were reason enough to reexamine the results in Table 4 and Fig. 14. The number of cycles at Blue Hill and Hanscom in Table 4 were decreased by 24 and 14%, respectively, to the nearest tenth of a cycle, and all the icing events were replotted in Fig. 16. The number of cycles for event number 7 was not adjusted because the detectors at Hanscom and Loon Mt. were switched after that icing event, but prior to the collection of additional data, to aid in correcting a minor wiring problem. The adjusted values presented in Fig. 16 do not affect the generally positive results of the field tests presented previously.

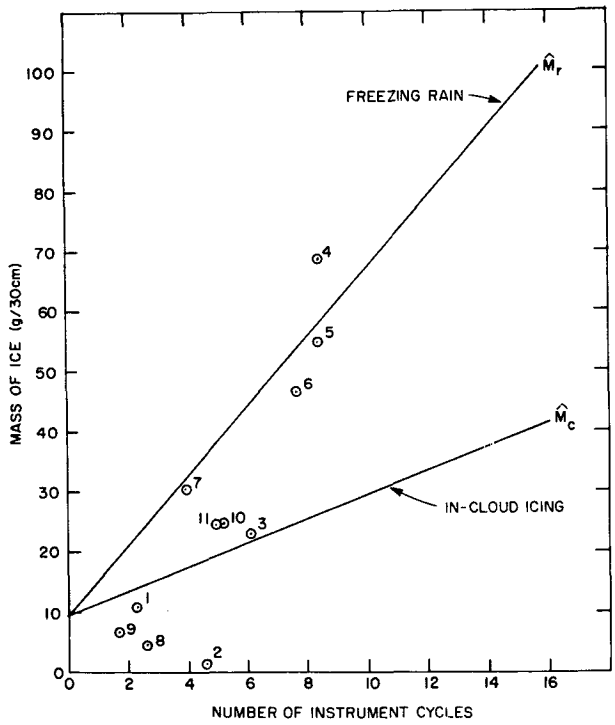

FIG. 16. Regression lines for the mass of ice measured on the 25-mm diameter cylinder vs the number of instrument cycles for freezing rain $\hat{M}_r$, and for in-cloud icing $\hat{M}_c$, based on the climatic chamber tests. Circled points represent the mass of ice measured on the cylinder vs the number of cycles for the field test icing events adjusted to compensate for instrument error. Event numbers from Table 4 identify each point.

8. Conclusions

Based on the analyses of the climatic chamber test data, and subsequent field tests, the Rosemount Model 872DC ice detection system has proved to be an effective tool for determining the mass and thickness of ice accretion on cylinders. Further field testing, especially at locations that favor in-cloud (rime) icing, is necessary to refine the relationships between the number of detector de-icing cycles and the mass and thickness of ice for different types and combinations of icing conditions.

The major hindrance to utilization of the detector "off-the-shelf" for making icing observations is the problem of retention of melt water on the flat surface area on top of the strut on which the sensor is located. This retained water can cause erroneous cycling upon refreezing. This situation occurs during light winds (≤15 knots). Since stronger winds blow the melt water off, it is not a problem during in-cloud icing, which requires fairly strong winds to blow supercooled droplets past a stationary surface to form ice.

The problem could be eliminated by tapering the top of the strut to facilitate drainage.

Although the main emphasis in this report has been on observing the quantity of ice resulting from a period of ice accretion, it is also important in engineering design to know the distribution of concurrent observations of wind and ice. Since strong windspeeds could occur subsequent to a period of icing, especially in cold locations, an observation program should include a method for determining the quantity of residual ice remaining on structures after the icing has ceased.

Acknowledgments. I would like to thank Richard Toliver, Wayne Drake, and their support group at the Armament Development and Test Center, Eglin AFB, Florida, for their close cooperation in the conduct of the climatic chamber tests. I am also grateful to Robert Skilling of the Blue Hill Observatory, John Govoni at the United States Army Cold Regions Research and Engineering Laboratory, to Arthur Kantor, Donald Grantham, Chien-hsuing Yang, Stuart Muench, William Lamkin and Stuart Sheets at AFGL for their support and to Helen Connell for typing this report.

REFERENCES

Ackley, S. F., K. Itagaki and M. Frank, 1973: An evaluation of passive deicing, mechanical deicing and ice detection. U.S. Dept. Transp., FAA-RD-74-50, Washington, DC, 50 pp.

Bennett, I., 1959: Glaze, its meteorology and climatology, geographical distribution and economic effects. Quartermaster Research and Engineering Center, Environ. Protection Res. Div., Tech. Rep. EP-105, Natick, MA, 217 pp.

Bilello, M. A., 1971: Frozen precipitation: its frequency and associated temperatures. Cold Regions Research and Engineering Laboratory, Hanover, NH, 13 pp.

Hill, A. N., 1973: An objective observation technique for freezing precipitation. Sterling Research and Development Center, Lab. Rep. No. 7-73, Sterling, VA, 25 pp.

Kuroiwa, D., 1965: Icing and snow accretion on electric wires. Cold Regions Research and Engineering Laboratory, Res. Rep. 123, Hanover, NH, 10 pp.

Lenhard, R. W., 1955: An indirect method for estimating the weight of glaze on wires. *Bull. Amer. Meteor. Soc.*, **36**, 1–5.

Macklin, W. C., 1961: The density and structure of ice formed by accretion. *Quart. J. Roy. Meteor. Soc.*, **88**, 30–50.

Mason, B. J., 1971: *The Physics of Clouds*, 2nd ed. Oxford University Press, 671 pp.

McKay, G. A., and H. A. Thompson, 1969: Estimating the hazard of ice accretion in Canada from climatological data, *J. Appl. Meteor.*, **8**, 927–935.

Rudneva, A. V., 1961: Glazed frost and ice formation on cables within the territory of the USSR. Aerospace Technology Division, Library of Congress, Special Translation, No. ATD U-64-47, 28 July 1964, 288 pp.

Stallabrass, J. R., and P. F. Hearty, 1967: The icing of cylinders in conditions of simulated freezing sea spray. National Research Council of Canada, Ottawa, 10 pp.

Tattelman, P., 1979: Climatic chamber tests of a surface ice accretion measurement system. Air Force Geophysics Laboratory, AFGL-TR-79-0079, AD A077022, Hanscom AFB, 50 pp.

——, and I. I. Gringorten, 1973: Estimated glaze ice and wind loads at the Earth's surface for the contiguous United States. Air Force Geophysics Laboratory, AFCRL-TR-73-0646, AD 775068, Hanscom AFB, 35 pp.